SI Appendix for

Hippocampal neurons' cytosolic and membrane-bound ribosomal mRNA profiles are differentially regulated by learning and subsequent sleep

James Delorme[1], Lijing Wang[1], Varna Kodoth[1], Yifan Wang[2,4], Jingqun Ma[3], Sha Jiang[1], Sara J. Aton[1#]

[1] Department of Molecular, Cellular, and Developmental Biology, University of Michigan, Ann Arbor, MI 48019

[2] Department of Computational Medicine and Bioinformatics, University of Michigan, Ann Arbor, MI 48019

[3] Bioinformatics Core, Biomedical Research Core Facilities, University of Michigan, Ann Arbor, MI 48019

[4] Present Address: Department of Health Sciences Research, Mayo Clinic, Rochester, MN 55905

This PDF file includes:

SI Materials and Methods

SI Figure Legends

Figures S1 to S11

Other SI materials for this manuscript include the following:

Datasets S1 – S11

SI Materials and Methods.

Mouse husbandry, handling, and behavioral procedures

All animal husbandry and experimental procedures were approved by the University of Michigan Institutional Animal Care and Use Committee (PHS Animal Welfare Assurance number D16-00072 [A3114-01]). For all studies, mice were maintained on a 12:12h light/dark cycle (lights on at 8 AM) with food and water provided *ad lib*. *B6.Cg-Tg(Camk2a-cre)T29-1Stl/J* mice (Jackson) were crossed to *B6N.129-Rpl22$^{tm1.1Psam}$/J* mice (Jackson) to express HA-tagged Rpl22 protein in Camk2a+ neurons. The resultant offspring thus expressed transgenes on a mixed C57Bl/6N and C57Bl6/J genetic background, due backcrossing of the two parent lines onto these two strains. Available data suggest that these parent mouse lines could show differences in phenotypes such as circadian rhythms and exploratory behaviors, which could in turn affect CFM measures. Offspring of crosses between these parent stains typically present with intermediate phenotypes for these features (1-5). Our mixed-background mice show SD-induced deficits in CFM consolidation, consistent with prior findings (6-10), as shown in **Figure S3**.

Double-transgenic mice were individually housed with beneficial enrichment for one week prior to experiments and were habituated to daily handling (5 min/day) for five days prior to experiments. For RNA seq experiments, mice were randomly assigned to one of four groups: HC + Sleep (n = 8), HC + SD (n = 7), CFC + Sleep (n = 8), CFC + SD (n = 7). Each mouse's bilateral hippocampi comprised one biological replicate for sequencing, and no samples were pooled between mice. Beginning at lights-on (8 AM), half of the mice underwent single-trial CFC as described previously (8, 11, 12). Briefly, at lights on (ZT 0) mice were placed in a novel conditioning chamber (Med Associates) and were allowed 2.5 min of free exploration time prior to delivery of a 2-s, 0.75 mA foot shock through the chamber's grid floor. After 3 min total in the chamber, mice were returned to their original home cage (HC). As a control for the effects of learning, HC controls remained in their home cage during this time. HC + SD or CFC + SD mice were then kept awake continuously by gentle handling (SD; consisting of cage tapping, nest disturbance, and if necessary, stroking with a cotton-tipped applicator) over the next 3 h for all RNA seq studies, or 5 h for all qPCR experiments. HC + Sleep and CFC + Sleep mice were permitted *ad lib* sleep in their home cage for the same time interval. For behavioral experiments to validate effects of SD on CFM consolidation in double-transgenic mice, CFC was carried out at ZT 0 as described above. Following CFC, mice were returned to their home cages and randomized into Sleep (n = 15) and SD (n = 13) groups. SD mice underwent a 6-h period of gentle handling SD, and were allowed subsequent recovery sleep in their home cage until ZT0 the

following day, at which point all mice were returned to the CFC chamber for CFM assessment, using previously-described methods (8, 9, 11, 12).

Translating Ribosome Affinity Purification (TRAP)

RiboTag TRAP was performed as previously described (13) by indirect conjugation (14), separating membrane-bound and free-floating ribosomes (15). Briefly, following 3 h *ad lib* sleep or SD, mice were sacrificed with an overdose of pentobarbital (Euthasol). Brains were extracted and bilateral hippocampi were dissected in ice cold dissection buffer (1x HBSS, 2.5 mM HEPES [pH 7.4], 4 mM $NaHCO_3$, 35 mM glucose, 100ug/ml cycloheximide). Each mouse's hippocampal tissue was then transferred to glass dounce column containing 1 ml homogenization buffer (10 mM HEPES [pH 7.4], 150 mM KCl, 10 mM $MgCl_2$, 2 mM DTT, 0.1 cOmplete™ Protease Inhibitor Cocktail [Sigma-Aldrich, 11836170001], 100 U/mL RNasin® Ribonuclease Inhibitors [Promega, N2111], and 100 µg/mL cycloheximide) and manually homogenized on ice. Homogenate was transferred to 1.5 ml LoBind tubes (Eppendorf) and centrifuged at 4°C at 1000 g for 10 min. The resulting supernatant (cytosolic fraction) was transferred to a new LoBind tube while the pellet (MB fraction) was resuspended in homogenization buffer. 10% NP40 was then added to the samples and incubated 5 min on ice, after which both MB and cytosolic fractions were centrifuged at 4°C at maximum speed for 10 min. The resulting supernatant from both MB and cytosolic fractions was then separated into Input (~50µL), Camk2a+ (~400µL), and pS6+ fractions (~500µL). For isolating ribosomes from Camk2a+ populations, fractions were incubated with 1:40 anti-HA antibody (Abcam, ab9110) (16). To isolate ribosomes from highly active (pS6+) neurons fractions were incubated with 1:25 anti-pS6 244-247 (ThermoFisher 44-923G) (17). Antibody binding of the homogenate-antibody solution occurred over 1.5 h at 4°C with constant rotation.

For affinity purification, 200 µl/sample of Protein G Dynabeads (ThermoFisher, 10009D) were washed 3 times in 0.15M KCl IP buffer (10 mM HEPES [pH 7.4], 150 mM KCl, 10 mM $MgCl_2$, 1% NP-40) and incubated in supplemented homogenization buffer (+10% NP-40). Following this step, supplemented buffer was removed, homogenate-antibody solution was added directly to the Dynabeads, and the solution was incubated for 1 h at 4°C with constant rotation. After incubation, the RNA-bound beads were washed four times in 900µL of 0.35M KCl (10mM HEPES [pH 7.4], 350 mM KCl, 10 mM $MgCl_2$, 1% NP40, 2 mM DTT, 100 U/mL RNasin® Ribonuclease Inhibitors [Promega, N2111], and 100 µg/mL cycloheximide). During the final wash, beads were placed onto the magnet and moved to room temperature. After removing the supernatant, RNA was eluted by vortexing the beads vigorously in 350 µl RLT (Qiagen, 79216). Eluted RNA was purified using RNeasy Micro kit (Qiagen).

Quantitative real-time PCR (qPCR)

For qPCR, RNA from each sample (i.e., bilateral hippocampi from one mouse) was converted into cDNA using the SuperScript IV Vilo Master Mix (Invitrogen 11756050). qPCR was performed on diluted cDNA that employed either Power SYBR Green PCR Mix (Invitrogen 4367659) or TaqMan Fast Advanced Master Mix (Invitrogen 4444557). For TRAP enrichment values, each sample was normalized to the geometric mean of *Pgk1* and *Gapdh* housekeeping transcripts and then normalized to the corresponding Input sample (TRAP enrichment = 2^(ΔCt_target - ΔCt_housekeeping). Effects of SD were assessed by normalizing all groups' expression to the HC + Sleep group. Effects of CFC were quantified by normalizing CFC + Sleep to HC + Sleep and normalizing CFC + SD to HC + SD. Primers for mRNAs quantified are listed below.

Target	**Forward Primer**	**Reverse Primer**
Gapdh	GTGTTTCCTCGTCCCGTAGA	AATCCGTTCACACCGACCTT
Pgk1	TCGTGATGAGGGTGGACTTC	ACAGCAGCCTTGATCCTTTG
Arc	CCAGATCCAGAACCACATGAA	GAGAGTGTACCCTCACTGTATTG
cFos	GAAGAGGAAGAGAAACGGAGAAT	CTTGGAGTGTATCTGTCAGCTC
Homer1a	GCATTGCCATTTCCACATAGG	ATGAACTTCCATATTTATCCACCT TACTT
Glua1	AGTGACGCTCGGGACCACAC	CTCTGGAAGGCCTCCGCCAT
Bdnf	GGTCACAGCGGCAGATAAA	TCAGTTGGCCTTTGGATACC
Hspa5	CCGAGAACACGGTCTTCGAT	ATTCCAAGTGCGTCCGATGA
Grin2a	CGTAGAGGATGCCTTGGTCA	CCATAGCCTGTGGTGGCAAA
Grin2b	CGGCCTGAGTGACAAGAAGT	TCCTCTCTGTGCTGCCATTG

Vglut1	CCAGCATCTCTGAGGAGGAG	GGCTGAGAGATGAGGAGCAG
Parv	GTCGATGACAGACGTGCTCA	TTGTGGTCGAAGGAGTCTGC
Sst	CTCGGACCCCAGACTCCGTC	CTCGGGCTCCAGGGCATCAT
Mbp	CCTTGACTCCATCGGGCGCT	CTTCTGGGGCAGGGAGCCAT
Gfap	TCCTGGAACAGCAAAACAAG	CAGCCTCAGGTTGGTTTCAT

Target	**Catalog # for ThermoFisher Taqman Probes**
Gapdh	Mm99999915_g1
Pgk1	Mm00435617_m1
FosB	Mm00500401_m1
ΔFosB	Custom-AP47Y2V
Homer1	Mm01282664_m1
Homer1a	Custom-APT2DGG
Atf3	Mm00476033_m1
Egr3	Mm00516979_m1
1700016P03Rik	Mm01253067_m1

RNA-seq and expression analysis

RNA-Seq was carried out at the University of Michigan's DNA Sequencing Core. Amplified cDNA libraries were prepared using Takara's SMART-seq v4 Ultra Low Input RNA Kit (Takara

634888) and sequenced on Illumina's NovaSeq 6000 platform. Libraries were run with onboard cluster generation, and together comprised 40% of a NovaSeq S4 200 cycle kit (v1.5; ~16–20 billion paired-end reads per flow cell, quality score ≥ 90% of bases higher than Q30). Sequencing reads (50 bp, paired-end) were mapped to *Mus musculus* using Star v2.6.1a and quality checked with Multiqc (v1.6a0). Reads mapped to unique transcripts were counted with featureCounts (18).

Differential expression analyses were run with Deseq2 on all 30 hippocampal samples, with bilateral hippocampi from each mouse constituting a biological replicate (19). Analyses were run with an initial filtering step (removing rows with < 10 counts) and with betaPrior = False. To test differences between subcellular fractions within their respective cell population, the design of the GLM was set to compare differences between supernatant and pellet-associated expression of transcripts. Camk2a+, pS6+, and Input samples were analyzed separately (e.g., Camk2a+[supernatant/pellet]). To quantify effects of SD and CFC on expression, the design was switched, and each cell population and subcellular fraction was analyzed separately. The same two-factor design was used to analyze the effects of an animal's state (Sleep or SD) and learning (CFC or HC) on RNA expression. The design compared the effects of SD alone by combining HC and CFC animals. This strategy accounted for differential effects of learning experiences on SD-driven changes to transcript profiles (20). SD-driven transcript changes identified with this strategy were compared with SD-driven changes in mRNA and proteins found in recent prior studies(21-23), as show in **Figure S5**. In contrast, the effect of learning (CFC) was assessed separately in CFC + Sleep and CFC + SD mice.

To characterize the differences between the effects of SD and CFC, significantly altered transcripts were analyzed using Ingenuity's Pathway Analysis (IPA). GO analyses were performed in IPA and DAVID's Functional Annotation tool. For subcellular fraction comparisons, 2000 of the top cytosolic (Log2FC > 0) and MB (Log2FC < 0) differentially-expressed transcripts (ranked by adjusted *p* values) were run through IPA's Canonical Pathways analysis. To characterize differences in common metabolic pathways between cytosolic and MB fractions, hierarchical clustering was used to visualize the most differentially-expressed transcripts. Since signaling pathways were less overlapping between the MB and cytosolic fraction, they were ranked by enrichment *p* values. Those transcripts were then run through DAVID's Functional Annotation tool, selecting for cellular composition to describe the cellular compartment the corresponding protein relates to. Data were plotted in Fragments Per Million (FPM) and their correlation value (R) calculated in the ViDger R package (24).

Immunohistochemistry

To characterize HA and pS6 expression in the hippocampus, experimentally naive animals were sacrificed and perfused with 1xPBS followed by 4% paraformaldehyde. 50μM coronal sections containing dorsal hippocampus were blocked in normal goat serum for 2 h and incubated overnight using a biotin conjugated anti-HA (Biolegend 901505, 1:500), anti-pS6 244-247 (ThermoFisher 44-923G, 1:500), and anti-parvalbumin (Synaptic Systems 195 004, 1:500) antibodies. Sections were then incubated with secondary antibodies - Streptavidin-Alexa Fluor® 647 (Biolegend 405237), Fluorescein (FITC) Goat Anti-Rabbit IgG (H+L) (Jackson 111-095-003), and Alexa Fluor® 555 Goat Anti-Guinea pig IgG H&L (Abcam ab150186). Immunostained sections were coverslipped in ProLong Gold Antifade Reagent (ThermoFisher, P36930) for imaging with a Leica SP5 laser scanning confocal microscope.

Supplementary Figure Legends.

Figure S1. Cytosolic and membrane protein-encoding transcripts are more abundant in supernatant and pellet ribosomal fractions, respectively. (A) Volcano plot of transcripts differentially expressed between pellet (red) and supernatant (blue) cell fractions of Camk2a+ neurons. Data are shown for n = 30 biological replicates from 30 total mice across the 4 treatment groups. Of the 28,071 transcripts detected, 7,651 (27%) were significantly (p_{adj} < 0.1) more abundant in the supernatant (cytosolic) fraction, and 10,911 (39%) were significantly more abundant in the pellet (MB) fraction. Complete transcript list in **Dataset S1**. **(B)** Volcano plot of transcripts differentially expressed between pellet (red) and supernatant (blue) cell fractions from pS6+ neurons. Of the 34,657 transcripts detected, 8,030 (23%) were significantly (p_{adj} < 0.1) enriched in the supernatant (cytosolic) fraction, and 14,244 (41%) were significantly enriched in the pellet (MB) fraction. Complete transcript list in **Dataset S2**. **(C-D)** Top 10 cellular component localizations (from DAVID) of the 2000 transcripts most differentially expressed (based on adjusted p value) between MB and cytosolic fractions from Camk2a+ **(C)** or pS6+ **(D)** neurons. **(E-F)** Top 20 most-enriched signaling and metabolic pathways represented by the 2000 most-differentially-expressed transcripts in Camk2a+ **(E)** or pS6+ **(F)** cytosolic or MB fractions. **(G)** Illustration of the synaptogenesis signaling pathway (IPA) protein components, with proteins' color coded to indicate corresponding transcripts' that are localized preferentially in cytosolic (red) and MB (blue) fractions of Camk2a+ neurons. Functional category analysis available in **Dataset S1.** **(H)** Log2FC values indicating differences in the abundance of transcripts for proteins in Creb1 signaling pathway, including upstream activators or inhibitors of Creb signaling, between the cytosolic and membrain fractions. Transcripts for pathway components selectively localized in the cytosolic or MB fractions of pS6+ neurons are shown in red and blue, respectively, with corresponding proteins subcategorized by encoded protein type. Functional category analysis available in **Dataset S2.**

Figure S2. Transcripts enriched in cytosolic and MB fractions from Input (whole hippocampus). (A) Volcano plot of transcripts significantly enriched in pellet (red) and supernatant (blue) cell fractions. Of the 27,773 transcripts detected, and 8,310 (30%) showed significant enrichment in the supernatant (cytosolic) fraction, 9,285 (33%) showed enrichment in the pellet (MB) fraction. Complete transcript list in **Dataset S3**. **(B)** Top 10 cellular component localizations (from DAVID) of the 2000 transcripts which were most significantly enriched (based on p_{adj} value) in either pellet (MB) or supernatant (cytosolic) fractions. **(C)** Top 20 most-enriched

signaling and metabolic pathways represented by the 2000 most-enriched transcripts in Input cytosolic or MB fractions. **(D)** Log2FC values indicating enrichment of transcripts from the ubiquitin signaling pathway in the cytosolic (red) or MB (blue) fractions. Functional category analysis available in **Dataset S3**

Figure S3. Post-CFC SD disrupts CFM consolidation in *B6N.129-Rpl22$^{tm1.1Psam}$/J × B6.Cg-Tg(Camk2a-cre)T29-1Stl/J* mice. ***Top:*** Experimental design. All mice underwent single-trial CFC at lights on (ZT 0) and were subsequently returned to their home cages; SD mice were kept awake via gentle handling over the first 6 h post-CFC. CFM was assessed 24 h later, as described previously(8, 9, 11, 12). ***Bottom:*** CFM consolidation was significantly disrupted in SD mice (n = 13), compared with mice allowed *ad lib* sleep (n = 15). * indicates p = 0.036, Student's t-test.

Figure S4. mRNAs altered by SD and prior learning on cytosolic ribosomes. ***Left*****:** Proportional and overlapping Venn diagrams of transcripts significantly altered by SD, CFC + Sleep, and CFC + SD in cytosolic fractions from Camk2a+ neurons, pS6+ neurons, and Input. ***Right:*** Volcano plots of Deseq2 results for transcripts measured in each condition.

Figure S5. Overlap of SD-altered transcripts with previously-characterized SD-altered mRNAs and proteins. Venn diagrams indicate degree of overlap for transcripts altered by SD in the present study and those previously reported for RNA seq of whole hippocampus following SD (Gaine et al., 2021) (21), for Camk2a+ TRAP-seq following SD (Lyons et al., 2020) (22), and for RNA seq and proteomics of whole forebrain synaptoneurosomes (characterizing transcripts which lose circadian rhythmicity in the context of SD; Noya et al., 2019) (23). Transcripts in each section are listed in **Dataset S11**.

Figure S6. Creb1 target transcripts are upregulated on cytosolic ribosomes after SD. (A) Z-scores for the 5 upstream transcriptional regulators whose target transcripts were most significantly affected by SD, ranked by p_{adj} values. **(B)** Networks of Creb1 transcriptional targets altered by SD in Camk2a+ (***top***) and pS6+ (***bottom***) neurons. Color of arrows from Creb1 to transcripts indicates the predicted direction of transcriptional regulation - orange (with red transcript symbols) denotes transcripts predicted to be upregulated by Creb1 which are upregulated following SD; blue (with green transcript symbols) indicates transcripts predicted to be repressed by Creb1 which are repressed by SD; yellow indicates SD-related changes that do not match predicted regulation by Creb1; grey indicates undermined effects of Creb1 on transcript

levels. **(C)** Relative Creb1 network regulation p_{adj} values and z-scores are plotted for cytosolic ribosomes' transcripts altered by SD, CFC + Sleep, and CFC + SD in Camk2a+ and pS6+ cell populations. Upstream regulator analysis results are included in **Dataset S9.** Cytosolic input CREB network analyses are available in **Figure S6**.

Figure S7. Input CREB upstream regulator analysis. Networks of Creb1 transcriptional targets altered by SD in the cytosolic fraction taken from whole hippocampal homogenate (Input). Color of arrows indicates predicted regulation by Creb1 following SD whereas the color of the gene symbol indicates Log_2 FC in expression following SD. Orange arrows pointing to red symbols indicates genes increased by Creb1 that are also increased by SD while blue arrows connote transcripts predicted to be repressed by Creb1 which are also repressed by SD. Yellow arrows encompass all SD-related changes that do not match predicted regulation by Creb1; grey indicates undetermined effects of Creb1 on transcript levels.

Figure S8. CFC-induced alterations in *Fosb* and *Homer1* splice variants are occluded by post-CFC SD in Camk2a+ neurons. (A) *Fosb* and *ΔFosb* expression for CFC and HC mice after 5 h of subsequent sleep or SD is shown for cytosolic fractions of the 3 cell populations. ***Top, left:*** Expression in the 4 conditions relative to values from HC + Sleep mice (Two-way ANOVA, CFC/SD, df = 18, *** p-value < 0.001). ***Top, right:*** Relative enrichment/de-enrichment for *Fosb* and *ΔFosb* in Camk2a+ and pS6+ neurons, relative to Input, for the 4 conditions. ***Bottom:*** Expression of Fosb and *ΔFosb* following CFC conditions relative to same-state (SD or Sleep) home-cage (HC) conditions (t-test, n = 5/group[HC], n = 6/group[CFC]) #, * , ** , and *** indicate $p < 0.1$, $p < 0.05$, $p < 0.01$, and $p < 0.001$, respectively. **(B)** *Homer1* and *Homer1a* in cytosolic fractions in the 4 conditions, normalized as described in **(A)**.

Figure S9. CFC-induced alterations in activity-dependent transcripts in Sleep and SD mice. Expression of activity-regulated transcripts *Cfos*, *Atf3*, *Arc*, and *Erg1*) and lncRNA *1700016P03Rik* for CFC and HC mice after 5 h of subsequent sleep or SD is shown for cytosolic fractions of Camk2a+ and pS6+ neurons. ***Top:*** Expression in the 4 conditions relative to values from HC + Sleep mice (Two-way ANOVA, CFC/SD, df = 18) *, **, and *** indicate $p < 0.05$, $p < 0.01$, and $p < 0.001$, respectively. ***Bottom:*** Expression for the CFC conditions relative to same-state (SD of Sleep) HC conditions.

Figure S10. mRNAs altered by SD and prior learning on MB ribosomes. *Left*: Proportional and overlapping Venn diagrams of transcripts significantly altered by SD, CFC + Sleep, and CFC + SD in MB fractions from Camk2a+ neurons, pS6+ neurons, and Input. ***Right:*** Volcano plots of Deseq2 results for transcripts measured in each condition.

Figure S11. Overview of data in Supplementary Datasets.

Supplementary Datasets.

Dataset S1 - Transcripts enriched in cytosolic or MB ribosomal fractions of Camk2a+ neurons.

Dataset S2 - Transcripts enriched in cytosolic or MB ribosomal fractions of pS6+ neurons.

Dataset S3 - Transcripts enriched in cytosolic or MB ribosomal fractions of Input.

Dataset S4 - Transcripts altered by SD and CFC in Camk2a+ neurons.

Dataset S5 - Transcripts altered by SD and CFC in pS6+ neurons.

Dataset S6 - Transcripts altered by SD and CFC in Input.

Dataset S7 - Venn diagram values.

Dataset S8 - Canonical/molecular functions altered by SD (cytosolic fractions).

Dataset S9 - CREB upstream regulator analysis (cytosolic fractions).

Dataset S10 - Canonical/molecular functions altered by SD and CFC (MB fractions).

Dataset S11 – Venn diagram values corresponding to Figure S4.

References Cited.

1. V. Kumar *et al.*, C57BL/6N mutation in Cytoplasmic FMR interacting protein 2 regulates cocaine response. *Science* **342**, 1508-1512 (2013).
2. S. L. Kirkpatrick *et al.*, Cytoplasmic FMR1-Interacting Protein 2 Is a Major Genetic Factor Underlying Binge Eating *Biol Psychiatry* **81**, 757-769 (2017).
3. C. D. Bryant *et al.*, Behavioral differences among C57BL/6 substrains: implications for transgenic and knockout studies *J Neurogenet* **22**, 315-331 (2008).
4. C. D. Bryant *et al.*, C57BL/6 substrain differences in inflammatory and neuropathic nociception and genetic mapping of a major quantitative trait locus underlying acute thermal nociception *Mol Pain* **15** (2019).
5. R. W. Corty, V. Kumar, L. M. Tarantino, J. S. Takahashi, W. Valdar, Mean-Variance QTL Mapping Identifies Novel QTL for Circadian Activity and Exploratory Behavior in Mice *G3 (Bethesda)* **8**, 3783-3790 (2018).
6. L. A. Graves, E. A. Heller, A. I. Pack, T. Abel, Sleep deprivation selectively impairs memory consolidation for contextual fear conditioning. *Learn. Mem.* **10**, 168-176 (2003).
7. C. G. Vecsey *et al.*, Sleep deprivation impairs cAMP signalling in the hippocampus. *Nature* **461**, 1122-1125 (2009).
8. N. Ognjanovski, C. Broussard, M. Zochowski, S. J. Aton, Hippocampal Network Oscillations Rescue Memory Consolidation Deficits Caused by Sleep Loss. *Cereb. Cortex* **28**, 3711-3723 (2018).
9. J. Delorme *et al.*, Sleep loss drives acetylcholine- and somatostatin interneuron-mediated gating of hippocampal activity, to inhibit memory consolidation. *Proc Natl Acad Sci USA* **118** (2021).
10. M. F. Qureshi, S. K. Jha, Short-Term Total Sleep-Deprivation Impairs Contextual Fear Memory, and Contextual Fear-Conditioning Reduces REM Sleep in Moderately Anxious Swiss Mice. *Front Behav Neurosci* **11** (2017).
11. N. Ognjanovski *et al.*, Parvalbumin-expressing interneurons coordinate hippocampal network dynamics required for memory consolidation. *Nature Communications* **8**, 15039 (2017).
12. N. Ognjanovski, D. Maruyama, N. Lashner, M. Zochowski, S. J. Aton, CA1 hippocampal network activity changes during sleep-dependent memory consolidation. *Front Syst Neurosci* **8**, 61 (2014).
13. E. Sanz *et al.*, Cell-type-specific isolation of ribosome-associated mRNA from complex tissues. *Proc Natl Acad Sci U S A* **106**, 13939-13944 (2009).
14. Y. Jiang *et al.*, Molecular profiling of activated olfactory neurons identifies odorant receptors for odors in vivo. *Nat Neurosci* **18**, 1446-1454 (2015).
15. A. Kratz *et al.*, Digital expression profiling of the compartmentalized translatome of Purkinje neurons. *Genome Res* **24**, 1396-1410 (2014).
16. T. Shigeoka, J. Jung, C. E. Holt, H. Jung, "Axon-TRAP-RiboTag: Affinity Purification of Translated mRNAs from Neuronal Axons in Mouse In Vivo" in RNA Detection (Methods in Molecular Biology). (Humana Press, New York, 2018), pp. 85-94.
17. Z. A. Knight *et al.*, Molecular profiling of activated neurons by phosphorylated ribosome capture. *Cell* **151**, 1126-1137 (2012).
18. Y. Liao, G. K. Smyth, W. Shi, featureCounts: an efficient general purpose program for assigning sequence reads to genomic features. *Bioinformatics* **30**, 923-930 (2013).
19. M. I. Love, W. Huber, S. Anders, Moderated estimation of fold change and dispersion for RNA-seq data with DESeq2. *Genome Biology* **15** (2014).
20. R. Havekes, S. J. Aton, Impacts of Sleep Loss Versus Waking Experience on Brain Plasticity: Parallel or Orthogonal? *Trends in Neuroscience* **43**, 385-393 (2020).

21. M. E. Gaine *et al.*, Altered hippocampal transcriptome dynamics following sleep deprivation *Mol Brain* **14** (2021).
22. L. C. Lyons, S. Chatterjee, Y. Vanrobaeys, M. E. Gaine, T. Abel, Translational changes induced by acute sleep deprivation uncovered by TRAP-Seq *Mol Brain* **13** (2020).
23. S. B. Noya *et al.*, The Forebrain Synaptic Transcriptome Is Organized by Clocks but Its Proteome Is Driven by Sleep *Science* **366** (2019).
24. A. McDermaid, B. Monier, J. Zhao, B. Liu, Q. Ma, Interpretation of differential gene expression results of RNA-seq data: review and integration. *Briefings in Bioinformatics* **20**, 2044-2054 (2019).

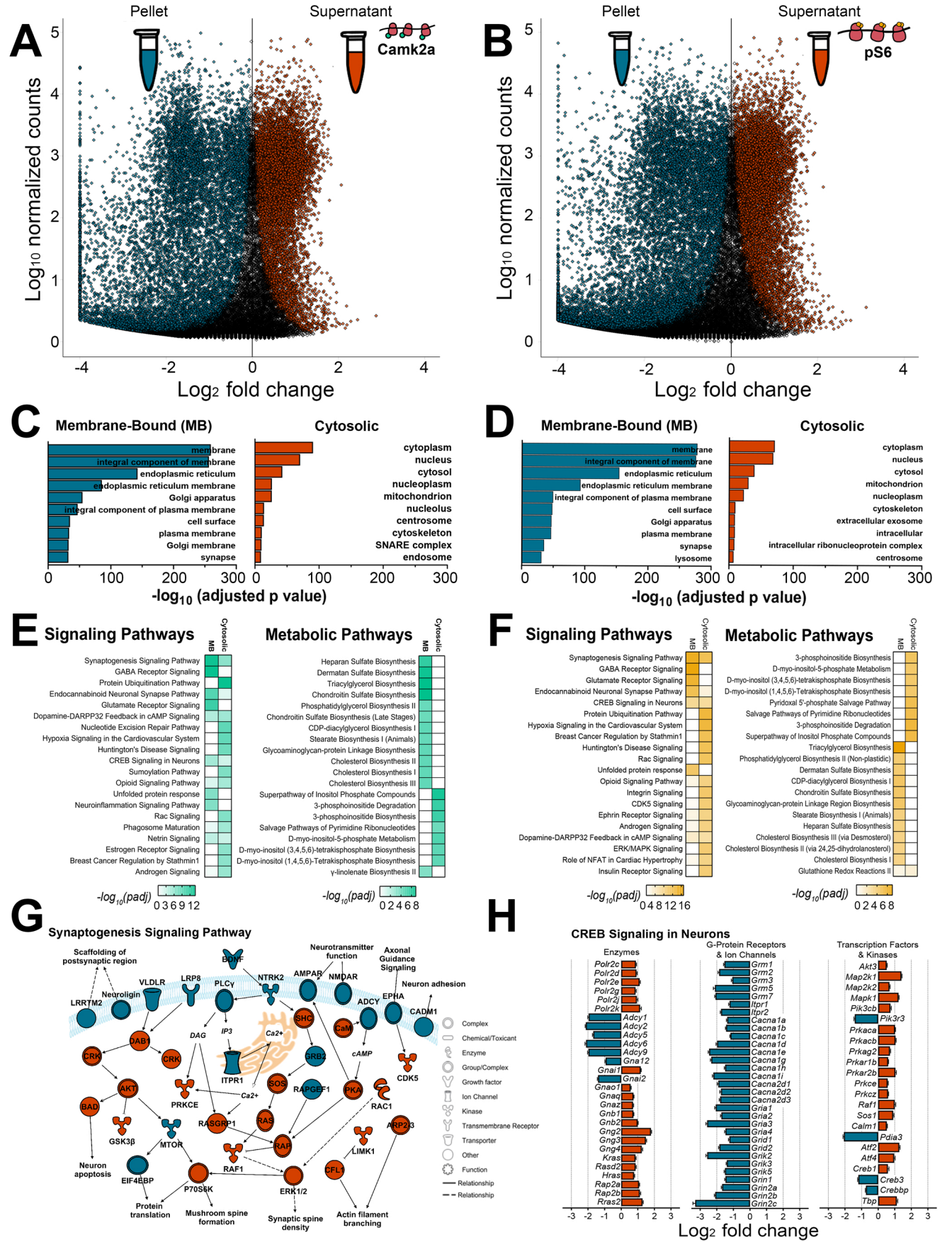
A
Pellet
Supernatant
Camk2a
Log10 normalized counts
Log2 fold change
B
Pellet
Supernatant
pS6
Log10 normalized counts
Log2 fold change
C
Membrane-Bound (MB)
membrane
integral component of membrane
endoplasmic reticulum
endoplasmic reticulum membrane
Golgi apparatus
integral component of plasma membrane
cell surface
plasma membrane
Golgi membrane
synapse
Cytosolic
cytoplasm
nucleus
cytosol
nucleoplasm
mitochondrion
nucleolus
centrosome
cytoskeleton
SNARE complex
endosome
-log10 (adjusted p value)
D
Membrane-Bound (MB)
membrane
integral component of membrane
endoplasmic reticulum
endoplasmic reticulum membrane
integral component of plasma membrane
cell surface
Golgi apparatus
plasma membrane
synapse
lysosome
Cytosolic
cytoplasm
nucleus
cytosol
mitochondrion
nucleoplasm
cytoskeleton
extracellular exosome
intracellular
intracellular ribonucleoprotein complex
centrosome
-log10 (adjusted p value)
E
Signaling Pathways
MB
Cytosolic
Synaptogenesis Signaling Pathway
GABA Receptor Signaling
Protein Ubiquitination Pathway
Endocannabinoid Neuronal Synapse Pathway
Glutamate Receptor Signaling
Dopamine-DARPP32 Feedback in cAMP Signaling
Nucleotide Excision Repair Pathway
Hypoxia Signaling in the Cardiovascular System
Huntington's Disease Signaling
CREB Signaling in Neurons
Sumoylation Pathway
Opioid Signaling Pathway
Unfolded protein response
Neuroinflammation Signaling Pathway
Rac Signaling
Phagosome Maturation
Netrin Signaling
Estrogen Receptor Signaling
Breast Cancer Regulation by Stathmin1
Androgen Signaling
-log10(padj)
0 3 6 9 12
Metabolic Pathways
MB
Cytosolic
Heparan Sulfate Biosynthesis
Dermatan Sulfate Biosynthesis
Triacylglycerol Biosynthesis
Chondroitin Sulfate Biosynthesis
Phosphatidylglycerol Biosynthesis II
Chondroitin Sulfate Biosynthesis (Late Stages)
CDP-diacylglycerol Biosynthesis I
Stearate Biosynthesis I (Animals)
Glycoaminoglycan-protein Linkage Biosynthesis
Cholesterol Biosynthesis II
Cholesterol Biosynthesis I
Cholesterol Biosynthesis III
Superpathway of Inositol Phosphate Compounds
3-phosphoinositide Degradation
3-phosphoinositide Biosynthesis
Salvage Pathways of Pyrimidine Ribonucleotides
D-myo-inositol-5-phosphate Metabolism
D-myo-inositol (3,4,5,6)-tetrakisphosphate Biosynthesis
D-myo-inositol (1,4,5,6)-Tetrakisphosphate Biosynthesis
γ-linolenate Biosynthesis II
-log10(padj)
0 2 4 6 8
F
Signaling Pathways
MB
Cytosolic
Synaptogenesis Signaling Pathway
GABA Receptor Signaling
Glutamate Receptor Signaling
Endocannabinoid Neuronal Synapse Pathway
CREB Signaling in Neurons
Protein Ubiquitination Pathway
Hypoxia Signaling in the Cardiovascular System
Breast Cancer Regulation by Stathmin1
Huntington's Disease Signaling
Rac Signaling
Unfolded protein response
Opioid Signaling Pathway
Integrin Signaling
CDK5 Signaling
Ephrin Receptor Signaling
Androgen Signaling
Dopamine-DARPP32 Feedback in cAMP Signaling
ERK/MAPK Signaling
Role of NFAT in Cardiac Hypertrophy
Insulin Receptor Signaling
-log10(padj)
0 4 8 12 16
Metabolic Pathways
MB
Cytosolic
3-phosphoinositide Biosynthesis
D-myo-inositol-5-phosphate Metabolism
D-myo-inositol (3,4,5,6)-tetrakisphosphate Biosynthesis
D-myo-inositol (1,4,5,6)-Tetrakisphosphate Biosynthesis
Pyridoxal 5'-phosphate Salvage Pathway
Salvage Pathways of Pyrimidine Ribonucleotides
3-phosphoinositide Degradation
Superpathway of Inositol Phosphate Compounds
Triacylglycerol Biosynthesis
Phosphatidylglycerol Biosynthesis II (Non-plastidic)
Dermatan Sulfate Biosynthesis
CDP-diacylglycerol Biosynthesis I
Chondroitin Sulfate Biosynthesis
Glycoaminoglycan-protein Linkage Region Biosynthesis
Stearate Biosynthesis I (Animals)
Heparan Sulfate Biosynthesis
Cholesterol Biosynthesis III (via Desmosterol)
Cholesterol Biosynthesis II (via 24,25-dihydrolanosterol)
Cholesterol Biosynthesis I
Glutathione Redox Reactions II
-log10(padj)
0 2 4 6 8
G
Synaptogenesis Signaling Pathway
Scaffolding of postsynaptic region
Neurotransmitter function
Axonal Guidance Signaling
Neuron adhesion
BDNF
NTRK2
AMPAR
NMDAR
PLCγ
LRP8
VLDLR
Neuroligin
LRRTM2
ADCY
EPHA
CADM1
SHC
CaM
DAB1
CRK
DAG
IP3
Ca2+
GRB2
cAMP
CDK5
ITPR1
SOS
RAPGEF1
PKA
AKT
PRKCE
RAC1
BAD
RASGRP1
RAS
ARP2/3
GSK3β
MTOR
RAF
LIMK1
Neuron apoptosis
EIF4EBP
RAF1
CFL1
P70S6K
ERK1/2
Protein translation
Mushroom spine formation
Synaptic spine density
Actin filament branching
Complex
Chemical/Toxicant
Enzyme
Group/Complex
Growth factor
Ion Channel
Kinase
Transmembrane Receptor
Transporter
Other
Function
Relationship
Relationship
H
CREB Signaling in Neurons
Enzymes
Polr2c
Polr2d
Polr2e
Polr2g
Polr2j
Polr2k
Adcy1
Adcy2
Adcy5
Adcy6
Adcy9
Gna12
Gnai1
Gnai2
Gnao1
Gnaq
Gnaz
Gnb1
Gnb2
Gng2
Gng3
Gng4
Kras
Rasd2
Hras
Rap2a
Rap2b
Rras2
G-Protein Receptors & Ion Channels
Grm1
Grm2
Grm3
Grm5
Grm7
Itpr1
Itpr2
Cacna1a
Cacna1b
Cacna1c
Cacna1d
Cacna1e
Cacna1g
Cacna1h
Cacna1i
Cacna2d1
Cacna2d2
Cacna2d3
Gria1
Gria2
Gria3
Gria4
Grid1
Grid2
Grik2
Grik3
Grik5
Grin1
Grin2a
Grin2b
Grin2c
Transcription Factors & Kinases
Akt3
Map2k1
Map2k2
Mapk1
Pik3cb
Pik3r3
Prkaca
Prkacb
Prkag2
Prkar1b
Prkar2b
Prkce
Prkcz
Raf1
Sos1
Calm1
Pdia3
Atf2
Atf4
Creb1
Creb3
Crebbp
Tbp
Log2 fold change

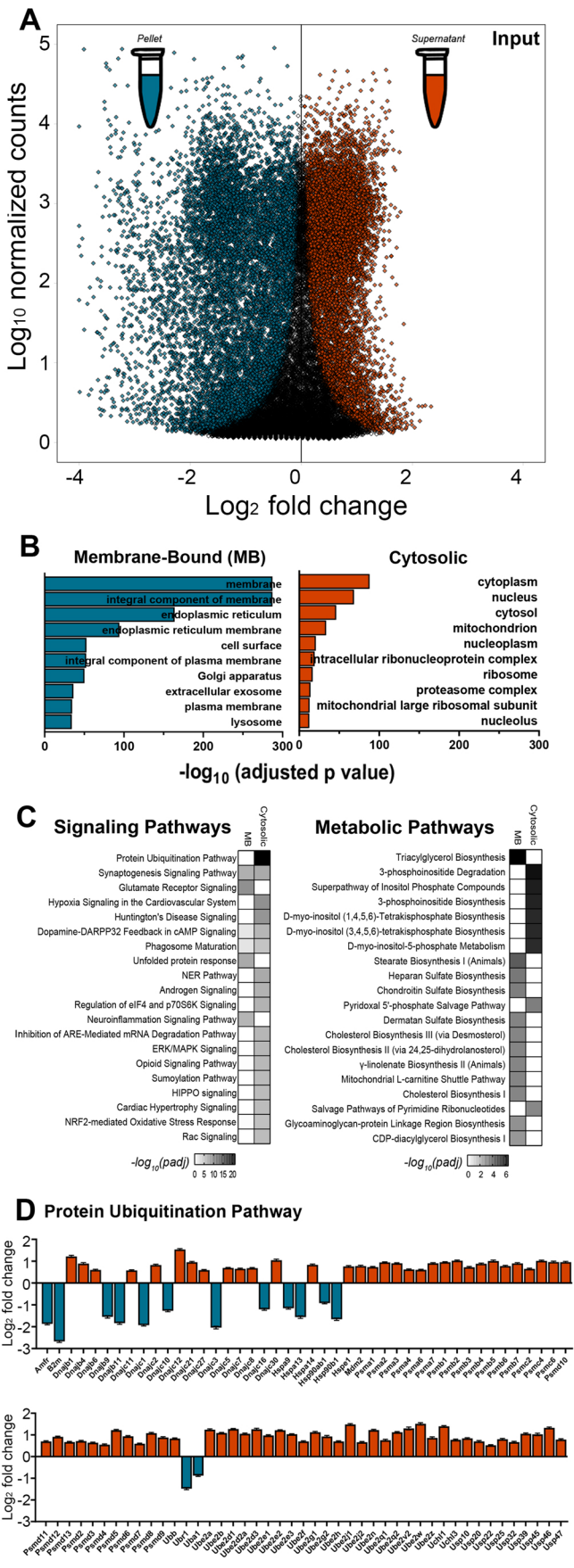
A
Pellet
Supernatant
Input
Log10 normalized counts
Log2 fold change
B
Membrane-Bound (MB)
membrane
integral component of membrane
endoplasmic reticulum
endoplasmic reticulum membrane
cell surface
integral component of plasma membrane
Golgi apparatus
extracellular exosome
plasma membrane
lysosome
Cytosolic
cytoplasm
nucleus
cytosol
mitochondrion
nucleoplasm
intracellular ribonucleoprotein complex
ribosome
proteasome complex
mitochondrial large ribosomal subunit
nucleolus
-log10 (adjusted p value)
C
Signaling Pathways
MB
Cytosolic
Protein Ubiquitination Pathway
Synaptogenesis Signaling Pathway
Glutamate Receptor Signaling
Hypoxia Signaling in the Cardiovascular System
Huntington's Disease Signaling
Dopamine-DARPP32 Feedback in cAMP Signaling
Phagosome Maturation
Unfolded protein response
NER Pathway
Androgen Signaling
Regulation of eIF4 and p70S6K Signaling
Neuroinflammation Signaling Pathway
Inhibition of ARE-Mediated mRNA Degradation Pathway
ERK/MAPK Signaling
Opioid Signaling Pathway
Sumoylation Pathway
HIPPO signaling
Cardiac Hypertrophy Signaling
NRF2-mediated Oxidative Stress Response
Rac Signaling
-log10(padj)
Metabolic Pathways
Triacylglycerol Biosynthesis
3-phosphoinositide Degradation
Superpathway of Inositol Phosphate Compounds
3-phosphoinositide Biosynthesis
D-myo-inositol (1,4,5,6)-Tetrakisphosphate Biosynthesis
D-myo-inositol (3,4,5,6)-tetrakisphosphate Biosynthesis
D-myo-inositol-5-phosphate Metabolism
Stearate Biosynthesis I (Animals)
Heparan Sulfate Biosynthesis
Chondroitin Sulfate Biosynthesis
Pyridoxal 5'-phosphate Salvage Pathway
Dermatan Sulfate Biosynthesis
Cholesterol Biosynthesis III (via Desmosterol)
Cholesterol Biosynthesis II (via 24,25-dihydrolanosterol)
γ-linolenate Biosynthesis II (Animals)
Mitochondrial L-carnitine Shuttle Pathway
Cholesterol Biosynthesis I
Salvage Pathways of Pyrimidine Ribonucleotides
Glycoaminoglycan-protein Linkage Region Biosynthesis
CDP-diacylglycerol Biosynthesis I
-log10(padj)
D
Protein Ubiquitination Pathway
Log2 fold change

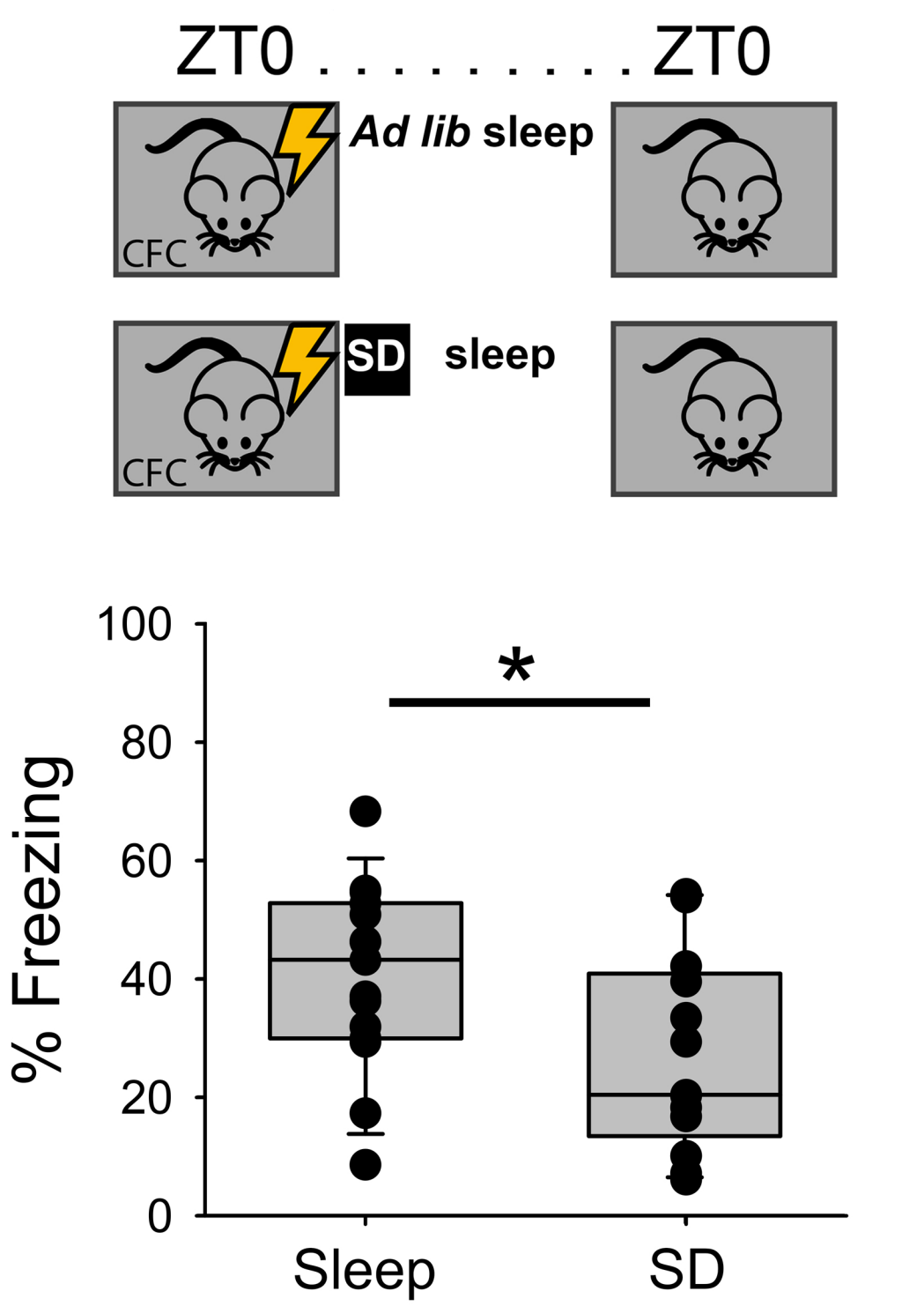
ZT0 . . . . . ZT0
Ad lib sleep
CFC
SD
sleep
CFC
100
80
60
40
20
0
% Freezing
*
Sleep
SD

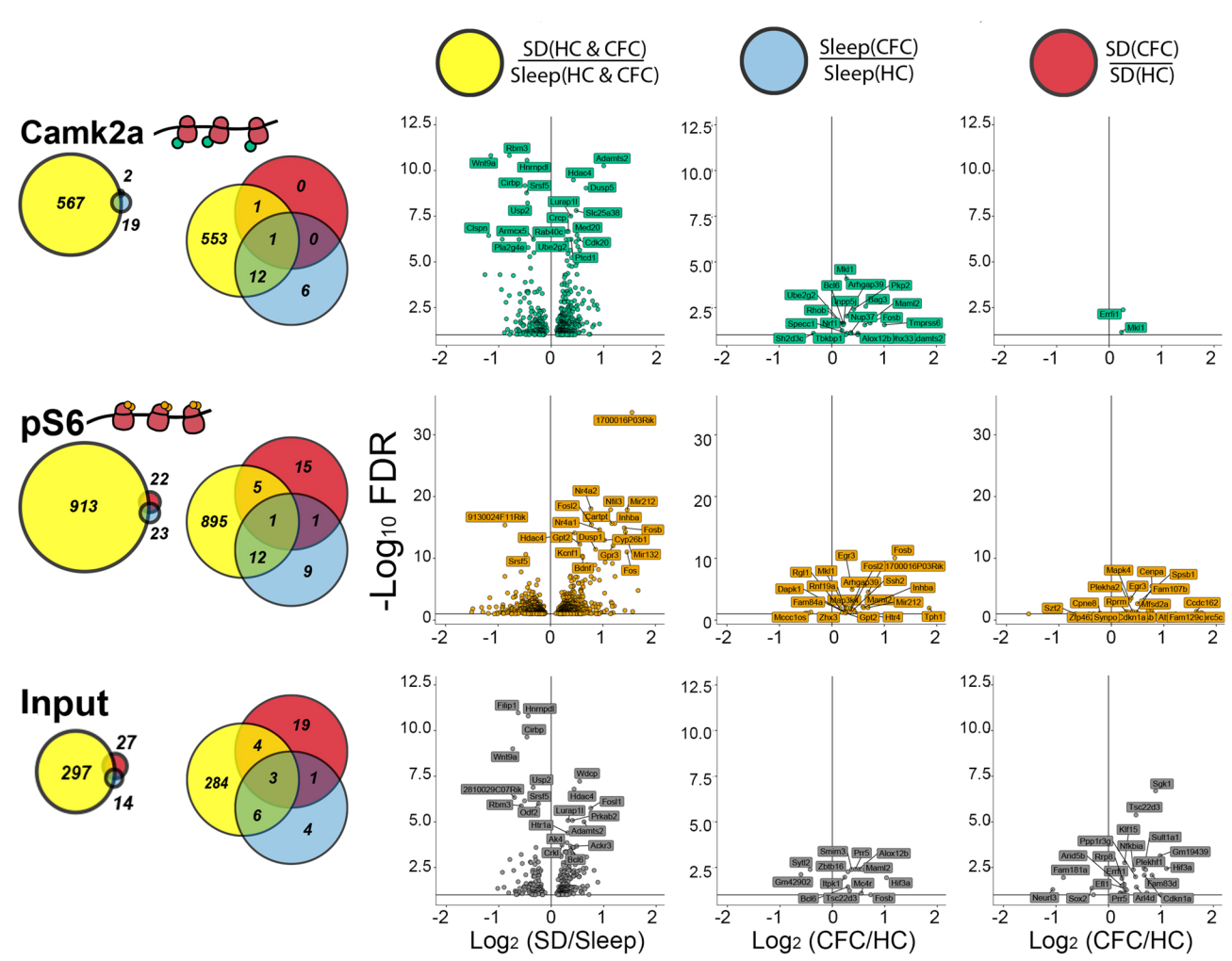
SD(HC & CF)
Sleep(HC & CF)
Sleep(CFC)
Sleep(HC)
SD(CFC)
SD(HC)
Camk2a
567
2
19
553
1
0
1
0
12
6
pS6
913
22
23
895
5
15
1
1
12
9
Input
297
27
14
284
4
19
3
1
6
4
-Log10 FDR
Log2 (SD/Sleep)
Log2 (CFC/HC)
Log2 (CFC/HC)

Input

Camk2a+

pS6+

Gaine et al., 2021(hippocampal transcripts)

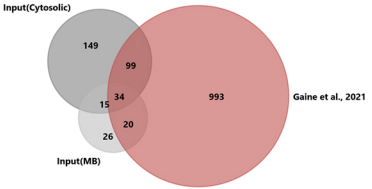

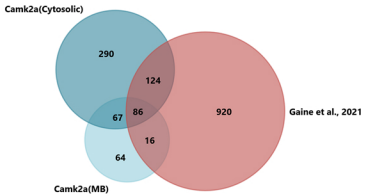

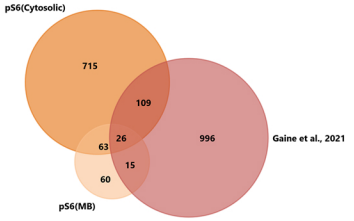

Lyons et al., 2020 (hippocampal Camk2a+ TRAP transcripts)

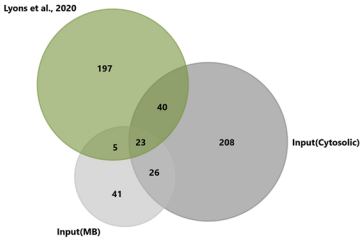

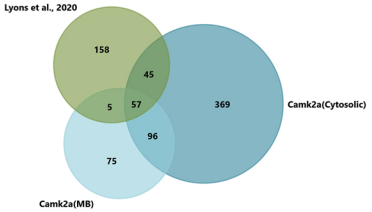

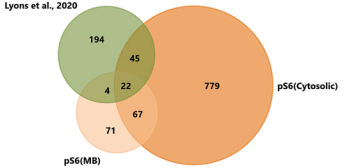

Noya et al., 2019 (forebrain synaptoneurosome transcripts)

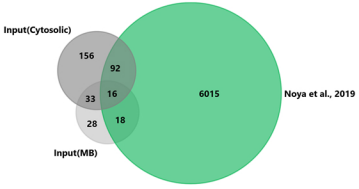

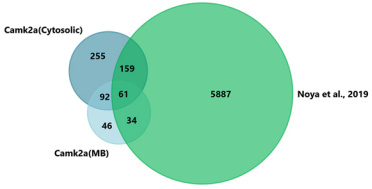

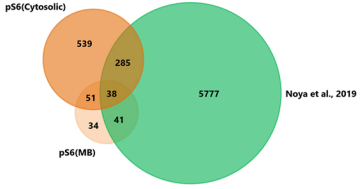

Noya et al., 2019 (forebrain synaptoneurosome proteins)

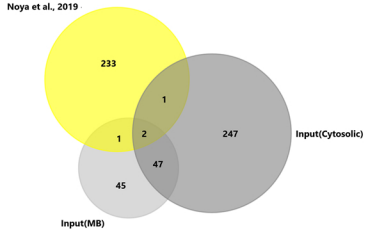

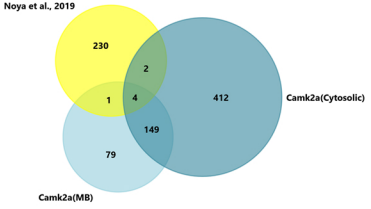

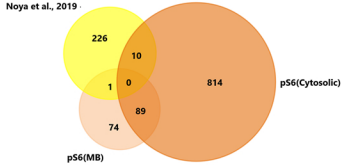

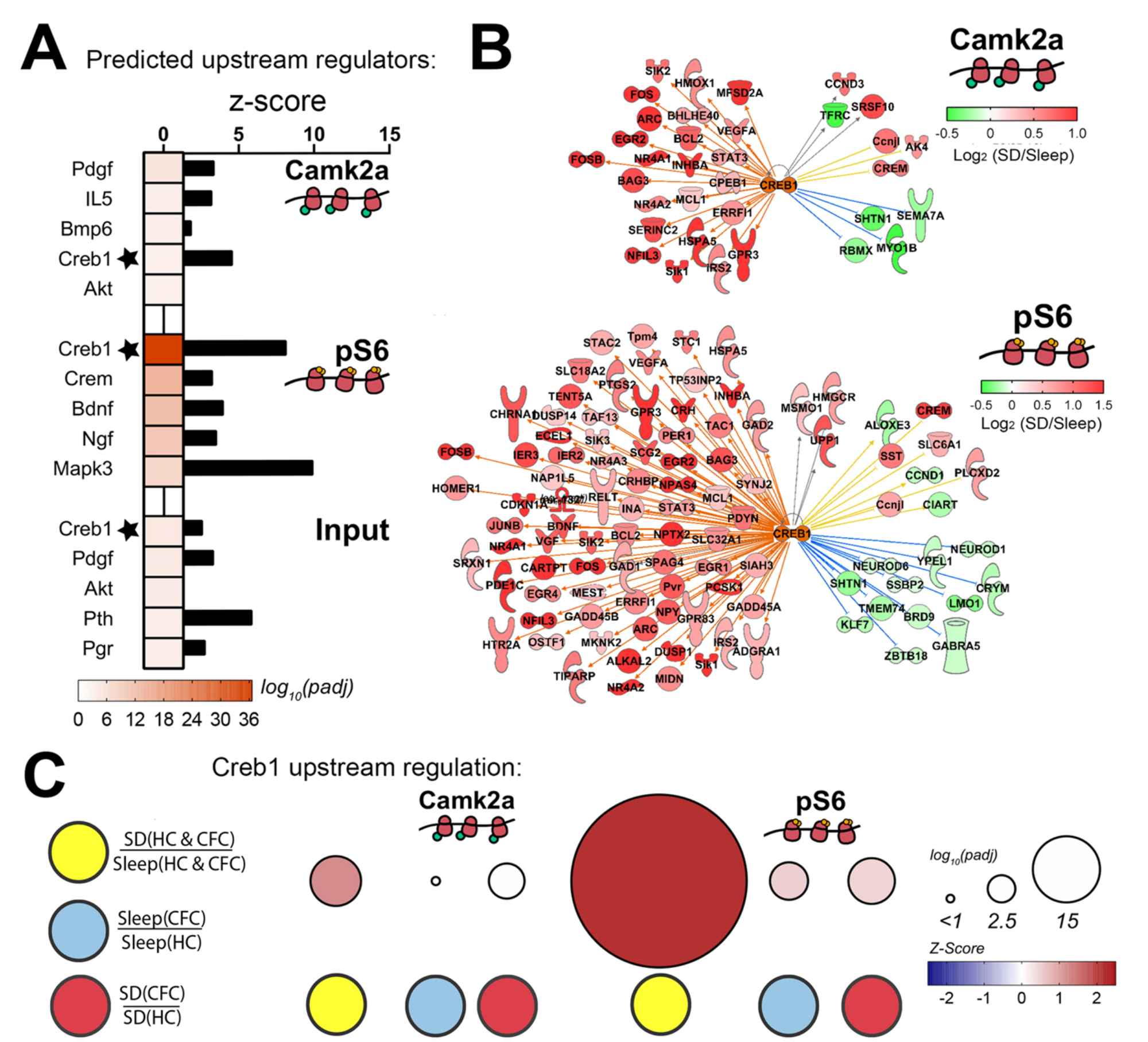
A
Predicted upstream regulators:
z-score
0
5
10
15
Pdgf
IL5
Bmp6
Creb1
Akt
Creb1
Crem
Bdnf
Ngf
Mapk3
Creb1
Pdgf
Akt
Pth
Pgr
Camk2a
pS6
Input
log10(padj)
0 6 12 18 24 30 36
B
Camk2a
-0.5 0 0.5 1.0
Log2 (SD/Sleep)
pS6
-0.5 0 0.5 1.0 1.5
Log2 (SD/Sleep)
C
Creb1 upstream regulation:
SD(HC & CFC)
Sleep(HC & CFC)
Sleep(CFC)
Sleep(HC)
SD(CFC)
SD(HC)
Camk2a
pS6
log10(padj)
<1 2.5 15
Z-Score
-2 -1 0 1 2

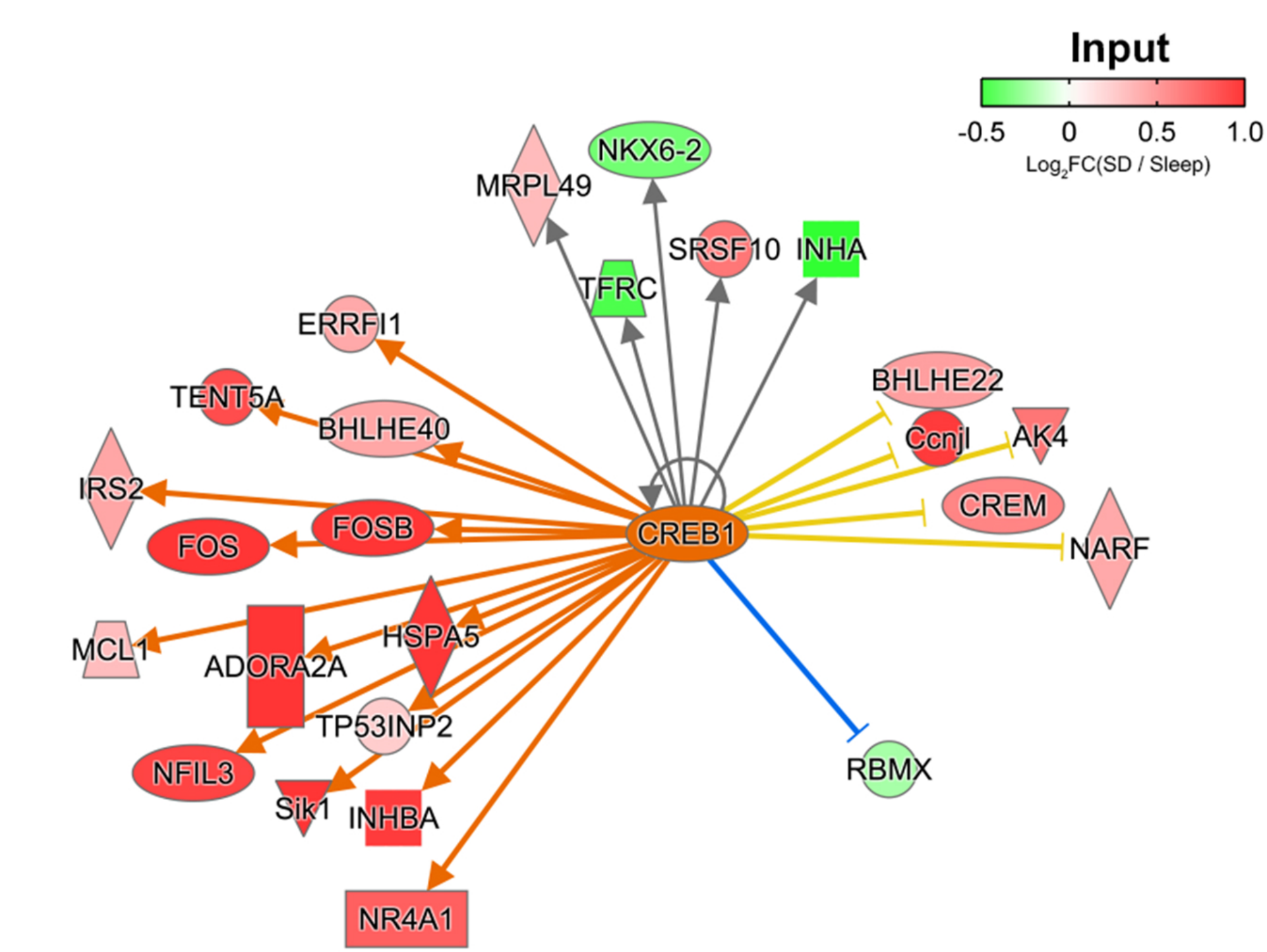
Input
-0.5
0
0.5
1.0
Log2FC(SD / Sleep)
NKX6-2
MRPL49
SRSF10
INHA
TFRC
ERRFI1
TENT5A
BHLHE40
BHLHE22
Ccnjl
AK4
IRS2
FOSB
FOS
CREB1
CREM
NARF
MCL1
ADORA2A
HSPA5
TP53INP2
NFIL3
Sik1
INHBA
RBMX
NR4A1

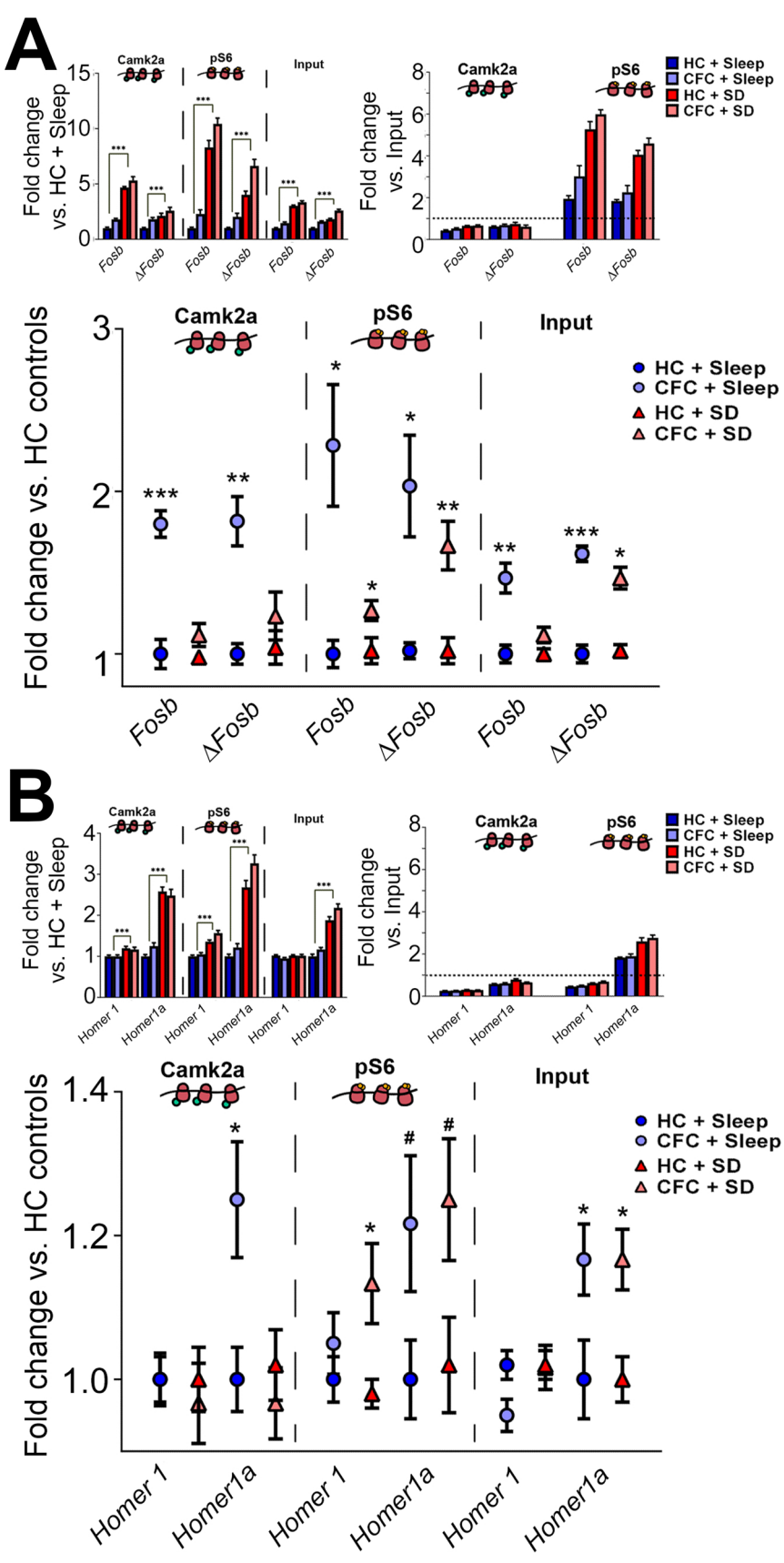
A
Camk2a
pS6
Input
Fold change vs. HC + Sleep
Fold change vs. Input
HC + Sleep
CFC + Sleep
HC + SD
CFC + SD
Fosb
ΔFosb
Fold change vs. HC controls
B
Homer 1
Homer1a

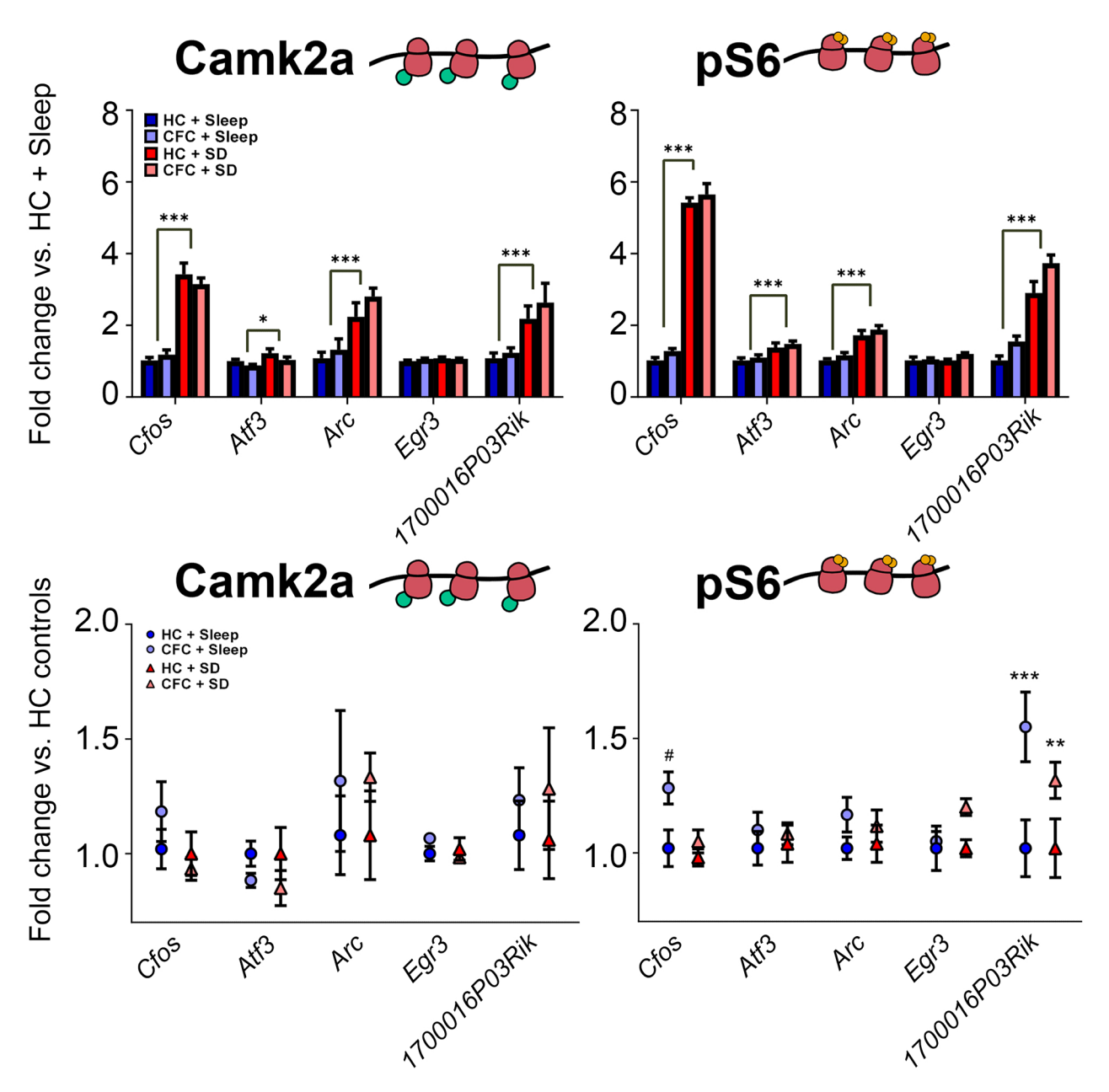
Camk2a
pS6
Fold change vs. HC + Sleep
HC + Sleep
CFC + Sleep
HC + SD
CFC + SD
Cfos
Atf3
Arc
Egr3
1700016P03Rik
Fold change vs. HC controls

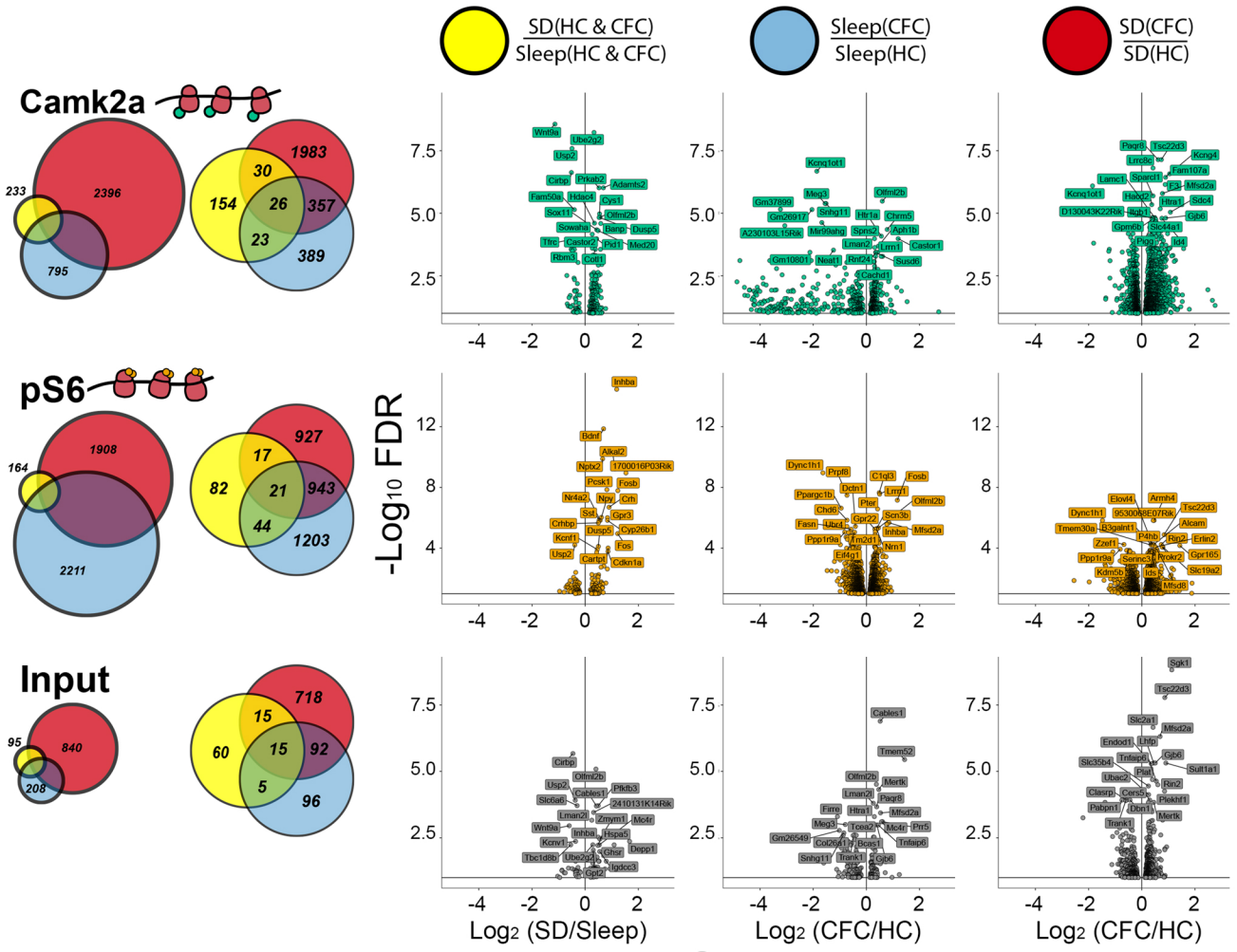
SD(HC & CFC)
Sleep(HC & CFC)
Sleep(CFC)
Sleep(HC)
SD(CFC)
SD(HC)
Camk2a
233
2396
795
1983
30
154
26
357
23
389
pS6
164
1908
2211
927
17
82
21
943
44
1203
Input
95
840
208
718
15
60
15
92
5
96
-Log10 FDR
Log2 (SD/Sleep)
Log2 (CFC/HC)
Log2 (CFC/HC)

Overview of Supplemental Tables

Supernatant vs. pellet:

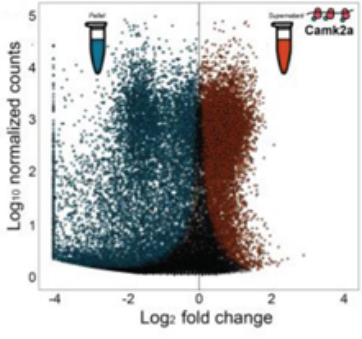

Camk2a+ Dataset S1

pS6+ Dataset S2

Input+ Dataset S3

SD vs. CFC:

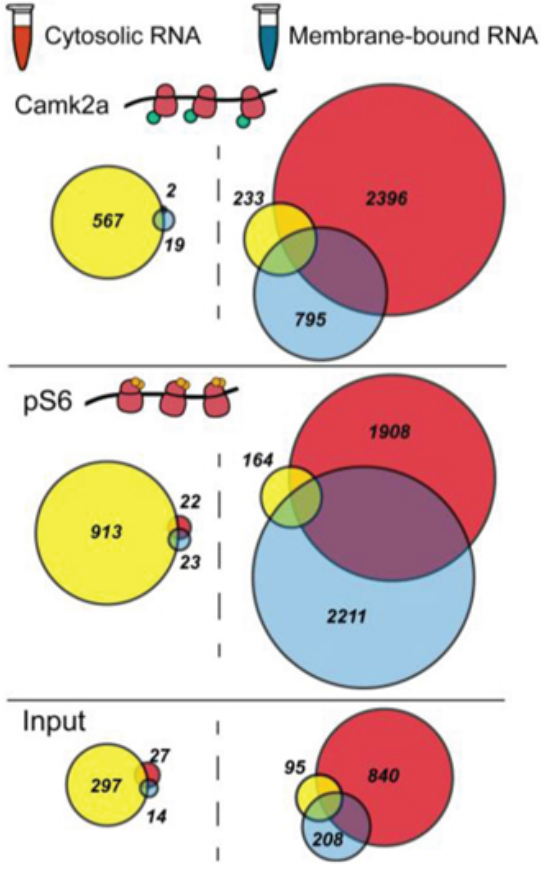

Camk2a+ Dataset S4

pS6+ Dataset S5

Input+ Dataset S6

Venn Overlap Transcripts (ALL) Dataset S7

Canonical/Molecular Functions (Cytosolic) Dataset S8

CREB UR Analysis (Cytosolic) Dataset S9

Canonical/Molecular Functions (MB) Dataset S10

Venn Overlap Transcripts with Prior Studies Dataset S11